High-resolution and multi-range particle separation by microscopic vibration in an optofluidic chip

Shi, Yu Zhi; Xiong, Sha; Chin, Lip Ket; Yang, Yi; Zhang, Jing Bo; Ser, Wee; Wu, Jiu Hui; Chen, Tian Ning; Yang, Zhen Chuan; Hao, Yi Long; Liedberg, Bo; Yap, Peng Huat; Zhang, Yi; Liu, Ai Qun

2017

Shi, Y. Z., Xiong, S., Chin, L. K., Yang, Y., Zhang, J. B., Ser, W., . . . Liu, A. Q. (2017). High-resolution and multi-range particle separation by microscopic vibration in an optofluidic chip. Lab on a Chip, 17(14), 2443-2450. doi:10.1039/c7lc00484b

https://hdl.handle.net/10356/139104

https://doi.org/10.1039/c7lc00484b

High-resolution and multi-range particle separation by microscopic vibration in an optofluidic chip

Y. Z. Shi,[ab] S. Xiong,*[b] L. K. Chin,[b] Y. Yang,[c] J. B. Zhang,[b] W. Ser,[b] J. H. Wu,[a]
T. N. Chen,[a] Z. C. Yang,[d] Y. L. Hao,[d] B. Liedberg,[e] P. H. Yap,[f] Y. Zhang*[g] and A. Q. Liu*[b]

[a] *School of Mechanical Engineering, Xi'an Jiao Tong University, Xian 710049, China*

[b] *School of Electrical and Electronic Engineering, Nanyang Technological University, Singapore 639798*

[c] *School of Physics and Technology, Wuhan University, Wuhan 430072, China*

[d] *National Key Laboratory of Science and Technology on Micro/Nano Fabrication, Institute of Microelectronics, Peking University, Beijing 100871, China*

[e] *School of Materials Science and Engineering, Nanyang Technological University, Singapore 639798*

[f] *Lee Kong Chian School of Medicine, Nanyang Technological University, Singapore 308232*

[g] *School of Mechanical and Aerospace Engineering, Nanyang Technological University, Singapore 639798*

* *Corresponding Author: xiongsha@ntu.edu.sg, yi_zhang@ntu.edu.sg, eaqliu@ntu.edu.sg*

Abstract

An optofluidic chip is demonstrated in experiments for the high-resolution and multi-range particle separation through the optically-induced microscopic vibration effect, where nanoparticles are trapped in loosely overdamped optical potential wells created with combined optical and fluidic constraints. It is the first demonstration of separating single nanoparticles with diameters ranging from 60 to 100 nm with a resolution of 10 nm. Nanoparticles vibrate with amplitude of 3–7 μm in the loosely overdamped potential wells in the microchannel. The proposed optofluidic device is capable of high-resolution particle separation at both nanoscale and microscale without reconfiguring the device. The separation of bacteria from other larger cells is accomplished using the same chip and operation condition. The unique trapping mechanism and the superb performance in high-resolution and multi-range particle separation of proposed optofluidic chip promise a great potential for a diverse range of biomedical applications.

Introduction

The ability to separate particles based on their different chemical and physical properties empowers a wide range of biomedical applications [1−3]. These particles could either be synthetic or natural. Synthetic particles, such as polystyrene microspheres, gold nanoparticles or quantum dots, are widely used to tag biomolecules for the sensing and sample processing [4, 5]. Naturally existing particles refer to cells, viruses or macromolecules such as large proteins. Separating pathogenic bacterial cells from human blood cells in clinical samples reduces the burden of background human genomic DNA hence increases the sensitivity of molecular diagnostics [6, 7]. Separating exosomes and other extracellular vesicles from cellular components allows for subsequent biomarker profiling and functional studies [8, 9]. For more integrated analysis, the particle separation process is often incorporated onto a microfluidic chip that utilizes various techniques, including immunoseparation [10], filtration [11], dielectrophoresis [12] and optical force [13], to distinguish and sort particles based on their different physical and chemical properties. One such important property for particle separation is the particle size. The particle separation device is usually configured to handle particles within a certain size range [14]. If a device is designed to separate nanoparticles from microparticles, it is unable to separate nanoparticles with small size difference from each other, and *vice versa*. Therefore, it is unfeasible to separate particles in different size ranges without reconfiguring the device.

One mechanism that has been widely used for particle separation is the non-invasive optical force [15]. However, the optical scattering and gradient forces increase with the 6^{th} and 3^{rd} powers of size, respectively [16]. When the size of a dielectric nanoparticle reduces to 200 nm, the optical scattering and

gradient forces become negligible. In the scenario of gold nanoparticles, an additional absorption force would act on the particles as a result of surface plasma resonance (SPR)-induced absorption of the light. The combined effect of the optical absorption force and the scattering force results in an optical extinction force, which could be enhanced by thousands of times when the light is under resonance. This enhanced force has been widely used to separate gold nanoparticles ranging from 100 to 200 nm [17−19]. Current methods for gold nanoparticle separation use the optical extinction force at a certain laser wavelength to push away the big particles (≥ 100 nm) while leaving the small particles unaffected. The separation resolution of this mechanism is limited to 30 nm for gold nanoparticles, which means particles with a size difference smaller than 30 nm cannot be distinguished using this approach. To separate even smaller nanoparticles (< 100 nm) using the optical extinction force requires a laser beam with a long propagating distance and a tight focus. If these conditions are not met, the optical force would be too small to manipulate nanoparticles as the intensity of the beam decays too quickly. Therefore, the separation of sub-100 nm gold nanoparticles with a high separation resolution remains a big challenge.

Optical chromatography, which utilizes the synergy of the optical scattering force and the fluidic drag force, has shown a great potential in nanoparticles separation [20]. Previous researches on optical chromatography demonstrated the sorting of microparticles with diameters of 1 to 3 μm [21, 22] and bacteria spores of ~ 1 μm in the longest dimension [23]. Optical chromatography can be developed into a chip scale device with the assistance of photonic crystal fibre [24]. The combination of hydrodynamic focusing and optical chromatography enables the sorting of sub-micron particles [25]. In order to separate sub-100 nm gold nanoparticles using optical chromatography, the light beam must have a tight focus (< 2

μm) so that the nanoparticles can be trapped in the potential well. If the focus is too big, the nanoparticles would escape easily [26–30]. Meanwhile, a small numerical aperture (NA) (< 0.05) is also necessary to separate gold nanoparticles with a small size difference (e.g. 10 nm). The tight focus and the small NA usually counteract each other for most beams such as the Gaussian beam. Therefore, designing light beams with a low NA (< 0.05) and a small beam spot (< 2 μm) is crucial for the separation of sub-100 nm gold nanoparticles with a high separation resolution (≤ 10 nm).

To address the aforementioned challenges, we demonstrate a quasi-Bessel be am with a low NA (~0.04) and a tight focus (< 0.5 μm) propagating against the flow stream in an optofluidic chip for the high-resolution and multi-range particle separation. Potential wells are created by building optical and fluidic constraints so that a single equilibrium position is defined for each particle of a unique size along the microchannel. The low divergence of the beam induces microscopic vibration (i.e. 3 to 7 μm) of nanoparticles inside the potential well. The microscopic vibration triggered by the Brownian force has not been observed in conventional optical trapping because such a stiffness (~10^{-10} N/m) is far lower than the safe trapping stiffness (>10^{-5} N/m). In our optofluidic chip, nanoparticles are trapped in the area of low stiffness because of optical and fluidic constraints. The microscopic vibration keeps each nanoparticle in its corresponding potential well and prevents nanoparticles in the closely positioned potential wells from aggregating. Using this approach, we are the first to demonstrate the separation of single gold nanoparticles ranging from 60 to 100 nm with a separation resolution of 10 nm in an optofluidic chip. This optofluidic chip is also capable of separating microscale particles without the need to change the device configuration. We demonstrate successful separation of bacteria from other larger cells using the same

operation conditions as those with gold nanoparticles on the same optofluidic chip. The ability of the proposed device to separate particles with high resolution and different size range promises great potentials for a diverse range of biomedical applications.

Design of the optofluidic chip

The optofluidic chip with hydrodynamic focusing and a quasi-Bessel beam is illustrated in Fig. 1(a). Gold nanoparticles were injected and confined to the central flow stream by hydrodynamic focusing. The quasi-Bessel beam was coupled into the flow stream in the microchannel by irradiating a fibre laser (NA = 0.12) through the micro-quadrangular lens built inside the optofluidic chip [31−33]. The micro-quadrangular lens can be regarded as the combination of two prisms with two open angles as shown in Fig. 1(b) and (c). The quasi-Bessel beam had a tightly focused main lobe (minimum 0.5 μm) and diverged slowly with an equivalent NA of 0.04. It also had a long propagating length over 140 μm as shown in Fig. 2(a). The nanoparticle in the microchannel experienced a dominant optical extinction force (F_{ext}) and a weak optical gradient force (F_{grad}) along the light propagation direction. Meanwhile, the nanoparticle was affected by the drag force (F_{drag}) along the flow stream direction. The powerful heating effect of the laser raised the temperature of the nanoparticle. As a result, the Brownian force (F_{bro}) plays an important role in the vibration of the nanoparticles [34]. Due to the combined effect of the heat absorption from the laser and the heat dissipation to the flow stream, the temperature distribution along the microchannel was non-uniform, resulting in a temperature gradient force (F_{Tg}).

At the equilibrium of these forces, the nanoparticle got trapped in the microchannel as shown in Fig. 2(b). The optical extinction force on the nanoparticle increased exponentially with the particle size while the drag force increased only linearly. Therefore, bigger nanoparticles were trapped in positions further away from the lens (z = 0) where the intensity was lower. Laser heating raised the temperature of the nanoparticles, whereas the flow streams facilitated the heat dissipation and cooled down the nanoparticles. The flow stream also absorbed the heat from the laser. The combined effect resulted in the temperature inhomogeneities along the microchannel as shown in Fig. 2(c). The influence of the Brownian force and the temperature gradient force (photophoretic force) were analysed based on the temperature distribution surrounding the nanoparticles.

Theoretical analysis

Due to its importance in force analysis, the temperature of the nanoparticles was calculated as a function of their diameters, laser intensities and flow rates. Rigorous simulations of energy transfer from the laser to the nanoparticles and further to the flow-stream were implemented in COMSOL. The spherical gold nanoparticle is placed in the de-ionized water with different flow rates under the illumination of different laser powers. The initial temperature of water and the environment is set to 293.15 K. The dimensions of the simulation region were 1 μm × 1 μm × 1 μm, and the maximum grid sizes for the surrounding medium and the gold nanoparticles were 10 nm and 1 nm, respectively. The temperature of the nanoparticles as a function of the diameter under the illumination with various laser intensities between 0.5 and 3 mW/μm^2 is shown in Fig. 3(a). The temperature increased with both the diameter and the laser intensity. At the laser

intensity of 2 mW/μm^2, an increase in diameter from 60 to 100 nm corresponded to a temperature increase from 364 to 387 K. When the laser intensity was 3 mW/μm^2, the temperature of all nanoparticles exceeded 397 K. In the experiments of sorting gold nanoparticles, the laser intensity is below 3 mW/μm^2. It causes the temperature of gold nanoparticles to increase by less than 100 kelvin, without evaporating the surrounding liquid. Evaporation happens only when the temperature is above the ultra-heat temperature, which is much higher than water boiling point of 373 K [35]. More importantly, the laser intensity is relatively low comparing to that used in previously reported tightly focused optical trapping experiments. The optimized laser power can effectively trap gold nanoparticles without damaging other microorganisms such as bacteria and protozoa in water [36]. In our optofluidic system, the temperature of the nanoparticles also decreased as the flow velocity increases as shown in Fig. 3(b). The temperature variation among nanoparticles with diameters ranging from 60 to 100 nm was smaller than 5 K when the flow velocity was relatively slow (i.e. $< 2 \times 10^{-1}$ m/s). The laser intensity used in the simulation was 1 mW/μm^2. And the flow velocity used in the experiments was in the order of 10^{-4} m/s. Therefore, the cooling effect caused by the flow-stream was ignored.

All forces acting on the nanoparticles with diameters ranging from 60 to 100 nm are shown in Fig. 3(c) when the laser intensity is 1 mW/μm^2 and the flow velocity is 10^{-4} m/s. The simulations were performed using the commercial software Lumerical. All forces acting on the nanoparticles increase with the nanoparticle diameter. Dipole resonance caused a distinct enhancement of the electric field on the nanoparticles and thus increased the optical extinction force, which was calculated using the Maxwell stress tensor method. The material parameters (dielectric function, ε) were obtained from Johnson and

Christy [37]. The optical extinction forces acting on the nanoparticles with a diameter of 60 nm and 100 nm were 0.043 pN and 0.099 pN, respectively. The drag force was expressed as $F_{drag} = 6\pi r\eta v$, where r was the radius of the nanoparticle, η was the viscosity of the liquid and v was the relative velocity of the nanoparticle and the flow stream. The drag force on the nanoparticle increased from 0.034 to 0.044 pN when the diameter increased from 60 to 100 nm, and v was 100 μm/s. The Brownian force on the nanoparticle was expressed as $F_{bro} = (2k_B T\gamma_f)^{1/2}\zeta(t)$, where k_B, T, γ_f and $\zeta(t)$ were the Boltzmann constant, the temperature of the nanoparticle, the drag coefficient and the normalised white noise, respectively. The expression $(2k_B T\gamma_f)^{1/2}$ increased from 3.41 to 4.40 fN when the diameter of the nanoparticle increased from 60 to 100 nm, as plotted in Fig. 3(c). The optical gradient force was proportional to the gradient of the light intensity. Because of the slow divergence of the quasi-Bessel beam, the gradient of the light intensity in the light propagation direction was small, which lead to a relatively small optical gradient force. The maximum optical gradient forces on nanoparticles with diameters between 60 and 100 nm ranged from 0.012 to 0.29 fN which were almost 100-fold smaller than the optical extinction force, drag force and Brownian force. Therefore, the gradient force along the light propagating direction was ignored. The temperature gradient drove the nanoparticles to the low-temperature region, in which the force was expressed as $F_{Tg} = -9\pi a\eta^2 H\Delta T/2\rho_f T$, where H, ΔT and ρ_f were the conductivity ratio between the gold (317 W/(m·K)) and the water (0.54 W/(m·K)), the temperature gradient and the density of the water, respectively [38]. Even when the temperature gradient was as large as 100 K, the temperature gradient force was in the order of 10^{-4} fN which was negligible. Therefore, the trapping of the nanoparticles was dominated by the optical extinction force, drag force and Brownian force. The three forces played different

roles in the manipulation of nanoparticles in the microchannel. The optical extinction force balanced with drag force to keep the nanoparticle trapped, while Brownian force triggered a microscopic vibration surround the equilibrium position due to the low divergence of the quasi-Bessel beam. The linear decay of the optical extinction force and constant fluidic drag force created optical and fluidic springs along the light propagating direction, which induced microscopic vibration. Given a constant laser power and flow rate, there was only a single position for the nanoparticle of each size where all forces reached equilibrium. The distance between the equilibrium position of a potential well and the micro-quadrangular lens was denoted as the trapping distance.

To trap a nanoparticle, the depth of the potential well should be at least 10 times greater than the kinetic energy of the Brownian motion [39, 40]. This criterion was expressed as $S = UT / k_B \geq 10$, where S was the stability number, U was the depth of the potential well, k_B was the Boltzmann constant and T was the temperature of the surroundings. Stability numbers of nanoparticles in an optical field with a laser power of 400 mW were calculated and plotted in Fig. 3(d). Nanoparticles with diameters smaller than 50 nm cannot be stably trapped in the microchannel due to their small stability numbers (S < 10). For nanoparticles with diameters larger than 80 nm, their stability numbers are always above 10, with a trapping distance of 140 μm from the micro-quadrangular lens. A nanoparticle with a diameter of 60 nm can only be stably trapped at a distance of 40 μm (S = 10.12). Determination of the stable trapping range is critical to the experimental trapping of different gold nanoparticles along the microchannel.

Experimental results and discussions

The optofluidic chip was fabricated using the soft-lithography processes. First, photoresist-on-silicon masters of the chips were prepared by photolithography (Micro-Chem, SU-8) using transparent glass masks (CAD/Art Services Inc., Poway, CA, USA). Then, the microchannels and the micro-quadrangular lens were moulded using PDMS and sealed against flat PDMS slabs after the oxygen plasma treatment. The microchannel had a refractive index of n = 1.405 and dimensions of L = 1000 μm, W = 70 μm and H = 50 μm. The microlens was made of PDMS and was placed at the edge of the microchannel. An argon ion laser (532 nm, Laser Quantum, mpc 6000) was coupled to a single mode optical fibre and inserted into the fibre groove near the microlens. Images were captured using an inverted optical microscope (TS 100 Eclipse, Nikon) through a charge-coupled device camera (Photron Fastcam SA3). The gold nanoparticles were dispersed in the water and injected into the microchannel using syringe pumps (Genie, Kent Scientific Corporation, CT, USA). For confocal imaging of the beam, the dye rhodamine 6G with a concentration of 1×10^{-7} mol/L (excitation: 532 nm, emission: 550–590 nm) was added to visualise the ray trajectories in the microchannel [41−43].

Separation of gold nanoparticles

The light-intensity profile of the quasi-Bessel beam used in the experiment is shown in Fig. 4(a). When the nanoparticles flowed into this optical field, nanoparticles of different sizes were trapped at different positions along the microchannel as shown in Fig. 4(b). The power used in this experiment was 400 mW and the flow rate was 300 μm/s. Nanoparticles with diameters of 60, 70, 80, 90 and 100 nm were trapped at different positions along the microchannel, i.e. at z = 32.5, 74.7, 104.6, 113.1 and 132 μm, respectively.

In Fig. 4(b), a single trapped nanoparticle with a diameter of 60 nm on the left in each frame served as a reference for the positions of larger nanoparticles to ensure that the trapping environment (e.g. laser power and flow rate) remains constant for each particle size. The trapping positions of the different particle sizes were also indicated by the white dashed lines in Fig. 4(a). Analysis of the various forces revealed that the optical extinction force and the drag force played the dominant roles in the trapping. Larger nanoparticles were trapped further from the lens (at which $z = 0$) because of the larger optical extinction forces. The results of this experiment showed that the nanoparticles were well separated based on their diameters without interference due to the self-healing property of the quasi-Bessel beam. In addition, the trapping positions of the nanoparticles in the microchannel were accurately predicted using the calculated optical extinction forces.

We calculated the trapping positions of the nanoparticles of variable sizes using the forces given by different stress tensors, and compared them with the measured positions (Detailed methods can be found in ESI†). The calculation of optical extinction forces on 60 – 100 nm gold nanoparticles with a laser intensity of 1 mW/μm^2 was shown in Fig. 5(a). The force calculated with the Minkooowski stress tensor was the biggest on each particle, while the smallest was the ones calculated using the Maxwell stress tensor. We calculated the trapping positions of nanoparticles using the forces given by different stress tensors, and compared them with the measured positions in the microchannel. As shown in Fig. 5(b), the measured results matched reasonably well with the results calculated using the Maxwell stress tensor for sizes of 60, 80, 90 and 100 nm. These experimental data were used to calibrate the functions relating the trapping positions of the nanoparticles to their diameters.

Separating of *E. coli* and *Cryptosporidium*

The optofluidic chip with a quasi-Bessel beam does not only have a high separation resolution for nanoparticles, but also separates microscale particles such as bacteria and protozoa efficiently under the same operation conditions. Fig. 6 shows the separation of *E. coli* and *Cryptosporidium* oocysts in the microchannel. *E. coli* (0.8–1.2 μm) and *Cryptosporidium* oocysts (4–6 μm) were trapped in the left and right clusters, respectively. The distance between the two groups of cells was approximately 160 μm. A single *E. coli* was observed moving to the left on the right side of *Cryptosporidium* oocysts cluster (t = 0). It was eventually trapped on the left of the microchannel at t = 6 s. In the meanwhile, another *E. coli* was moving towards left. And more *E. coli* was continuously trapped on the left and generates a cluster (t = 12 s). The separation of these microscale particles was performed under the same operation conditions as the experiment with gold nanoparticles. This optofluidic chip is capable of separating micro- and nano particles of different size ranges in the microchannel without device reconfiguration.

Vibration of trapped gold nanoparticles

The effect of the optical field on the nanoparticle is approximated by a harmonic potential well [44−47]. Experiments involving optical trapping are often conducted in liquids with viscosities of approximately 10^{-3} Pa·s, in which the system is overdamped [48−50]. The combination of the low divergence of the quasi-Bessel beam and the microfluidic flow creates loosely overdamped potential wells ($\omega_0 << 1/2\tau_p$) with an optical trapping stiffness of ~ 10^{-10} N/m inside the microchannel. In a typical tightly overdamped

system (stiffness $k = 10^{-5}$–10^{-4} N/m) [42, 43], the Brownian motion of the nanoparticles is confined to a displacement of 100 nm. The loosely overdamped system ($k = 10^{-10}$–10^{-9} N/m) generated by the quasi-Bessel beam makes the nanoparticle vibrate within a displacement in the micron scale. This displacement magnitude is explained by the Langevin equation for the kinetics of Brownian particles, i.e. $m_e \ddot{x}(t) + \gamma_{flow} \dot{x}(t) + Kx(t) = F_{th}(t) + F_{ext}$, where F_{th} and F_{ext} are the thermal and external forces on the nanoparticle, respectively. The mean square displacement (MSD) of the nanoparticle in an overdamped potential well is expressed as [51]

$$MSD(t) = \frac{1}{m_p \omega_0^2 \gamma} \left[1 - \frac{1}{2|\omega_1|\psi'_+} e^{-t/\psi'_-} + \frac{1}{2|\omega_1|\psi'_-} e^{-t/\psi'_+} \right], \quad (1)$$

where $\omega_1 = \sqrt{\omega_0^2 - (1/2\tau_p)^2}$ is the corner frequency, and $\psi'_\pm = 2\tau_p / (1 \pm 2\tau_p |\omega_1|)$. In the experiments, the trapping stiffness for the nanoparticles with a diameter of 60 nm was -2.45×10^{-10} N/m, and the resultant mean displacement of the nanoparticles was approximately 7.1 μm which was consistent with the calculated square root of the MSD, 7.31 μm. More calculation of nanoparticle vibration can be found in ESI†.

The experimental observation of microscopic vibration is shown in Fig. 7. The extremely small trapping stiffness of the potential wells is created by two constraints, one on each side of the well. The optical constraint on one side is created by the dominating extinction force, and the fluidic constraint on the other side is created by the drag force. With the two constraints, even a trapping stiffness as low as 10^{-10} N/m is able to confine the nanoparticle within the two constraints. When the nanoparticle is on the left side of the equilibrium position of optical and drag forces, the constraint of the optical force pushes

the nanoparticle back to the equilibrium position. When the nanoparticle is on the right side of the equilibrium position, the constraint of the drag force becomes the dominating factor and again pushes the nanoparticle back to the equilibrium position. The particle vibrates due to the Brownian motion, while Stokes viscous drag acts on the particle throughout the process. However, once a nanoparticle is trapped inside a potential well, it can only vibrate within a certain distance because of the constraints. The potential well for the larger particle is positioned at a location with a larger optical extinction force, resulting in a higher trapping stiffness. Therefore, the vibration of the nanoparticle is confined to a shorter displacement (right side of the beam in Fig. 7). More analysis can be found in ESI†. In the experiment, a 100-nm nanoparticle was trapped on the right of a 60-nm nanoparticle. The 100-nm nanoparticle vibrated due to the Brownian force, with a displacement of 6.3 μm during an average period of 6 s. The 60-nm nanoparticle vibrated with a displacement of approximately 7.1 μm, and appeared brighter than the 100-nm particle, because the optical intensity was much stronger near the lens and the resonance peak of the 60-nm particle (544 nm) was closer to the laser wavelength (532 nm) compared with that of the 100-nm particle (574 nm). When the resonance peak of gold nanoparticles is close to the laser wavelength, strong localized surface plasma resonance (LSPR) is induced, which enhances the optical extinction force by hundreds fold comparing to that on non-metallic nanoparticles. The LSPR enhanced optical extinction force acting on a 60-nm gold nanoparticle can balance the drag force under the flow velocity of 300 μm/s. On the contrary, non-metallic nanoparticles (< 100 nm) can hardly be trapped due to the extremely small optical force when the flow velocity is higher than 10 μm/s. Since the optical extinction force increases

as the sixth power of the size of the nanoparticle, this approach could be used to separate 200 and 300 nm polystyrene nanoparticles with a flow velocity of 50−100 μm/s.

Conclusions

In conclusion, for the first time, gold nanoparticles with diameters from 60 to 100 nm were separated with a separation resolution of 10 nm using isolated optical potential wells in an optofluidic chip. The potential wells were created along the microchannel by combining optical and fluidic forces to trap nanoparticles at specific positions. The nanoparticles vibrated with large displacements (3–7 μm) in the loosely overdamped optical potential wells which had a trapping stiffness of 10^{-10}–10^{-9} N/m. The optical trapping force and the microscopic vibration of gold nanoparticles were modelled, and the modelling results were consistent with the experimental results. The observed microscopic vibration facilitated the separation of nanoparticles with similar sizes by preventing them from aggregating. In addition, the optofluidic chip separated particles of different size ranges in the microchannel under the same operation condition. It was used to separate bacteria from larger cells. The high-resolution and multi-range particle separation represents a promising technology for various biomedical applications that require an accurate size-selective control of multi-scale particles.

Acknowledgements

This work was supported by Singapore National Research Foundation under the Competitive Research Program (NRF-CRP13-2014-01), and under the Incentive for Research & Innovation Scheme (1102-IRIS-05-02) administered by PUB.

References

[1] P. Sajeesh and A. K. Sen, *Microfluidics and Nanofluidics*, 2014, **17**, 1−52.

[2] L. R. Huang, E. C. Cox, R. H. Austin and J. C. Sturm, *Science*, 2004, **304**, 987−990.

[3] X. Ding, Z. Peng, S.-C. S. Lin, M. Geri, S. Li, P. Li, Y. Chen, M. Dao, S. Suresh and T. J. Huang, *Proc. Natl. Acad. Sci. U.S.A.*, 2014, **111**, 12992−12997.

[4] K. Saha, S. S. Agasti, C. Kim, X. N. Li and V. M. Rotello, *Chem. Rev.*, 2012, **112**, 2739−2779.

[5] J. P. Lafleur, S. Senkbeil, T. G. Jensen and J. P. Kutter, *Lab Chip*, 2012, **12**, 4651−4656.

[6] H. Fukushima, K. Katsube, Y. Hata, R. Kishi and S. Fujiwara, *Appl. Environ. Microbiol.*, 2007, 73, 92−100.

[7] I.-F. Cheng, H.-C. Chang, T.-Y. Chen, C. Hu and F.-L. Yang, *Sci. Rep.*, 2013, **3**, 2365.

[8] B. H. Wunsch, J. T. Smith, S. M. Gifford, C. Wang, M. Brink, R. L. Bruce, R. H. Austin, G. Stolovitzky and Y. Astier, *Nat. Nanotech.*, 2016, **11**, 936−940.

[9] K. E. Petersen, E. Manangon, J. L. Hood, S. A. Wickline, D. P. Fernandez, W. P. Johnson and B. K. Gale, *Anal. Bioanal. Chem.*, 2014, **406**, 7855−7866.

[10] E. T. Leary, T. Wang, D. J. Baker, D. D. Cilla, J. Zhong, G. R. Warnick, K. Nakajima and R. J. Havel, *Clin. Chem.*, 1998, **44**, 2490–2498.

[11] D. Di Carlo, J. F. Edd, D. Irimia, R. G. Tompkins and M. Toner, *Anal. Chem.*, 2009, **55**, 24−34.

[12] P. R. C. Gascoyne and J. Vykoukal, *Electrophoresis*, 2002, **23**, 1973−1983.

[13] M. P. MacDonald, G. C. Spalding and K. Dholakia, *Nature*, 2003, **426**, 421−424.

[14] L. Ren, Y. Chen, P. Li, Z. Mao, P.-H. Huang, J. rufo, F. Guo, L. Wang, J. P. McCoy, S. J. Levine and T. J. Huang, *Lab Chip*, 2015, **15**, 3809−3954.

[15] A. Ashkin, J. M. Dziedzic, J. E. Bjorkholm and S. Chu, *Opt. Lett.*, 1986, **11**, 288−290.

[16] K. C. Neuman and A. Nagy, *Nat. Methods*, 2008, **5**, 491−505;

[17] A. Cuche, A. Canaguier-Durand, E. Devaux, J. A. Hutchison, C. Genet and T. W. Ebbesent, *Nano Lett.*, 2013, **13**, 4230−4235.

[18] M. Ploschner, T. Cizmar, M. Mazilu, A. Di Falco and K. Dholakia, *Nano Lett.*, 2012, **12**, 1923−1927.

[19] W. Wu, X. Zhu, Y. Zuo, L. Liang, S. Zhang, X. Zhang and Y. Yang, *ACS Photonics*, 2016, **3**, 2497−2504.

[20] T. Kaneta, Y. Ishidzu, N. Mishima and T. Imasaka, *Anal. Chem.*, 1997, **69**, 2701−2710.

[21] T. Imasaka, Y. Kawabata, T. kaneta and Y. Ishidzu, *Anal. Chem.*, 1995, **67**, 1763−1765.

[22] S. J. Hart, A. V. Terray, K. L. Kuhn, J. Arnold and T. A. Leski, *Proceedings of the SPIE*, 2004, **5514**, 35−47.

[23] S. J. Hart, A. Terray, T. A. Leski, J. Arnold and R. Stroud, *Anal. Chem.*, 2006, **78**, 3221−3225.

[24] P. C. Ashok, R. F. Marchington, P. Mthunzi, T. F. Krauss and K. Dholakia, *Opt. Express*, 2010, **18**, 6396−6407.

[25] A. Terray, C. G. Hebert and S. J. Hart, *Biomicrofluidics*, 2014, **8**, 064102.

[26] L. K. Chin, A. Q. Liu, X. M. Zhang, C. S. Lim, J. H. Ng, J. Z. Hao and S. Takahashi, *Appl. Phys. Lett.*, 2007, **91**, 243901.

[27] Y. Yang, A. Q. Liu, L. K. Chin, X. M. Zhang, D. P. Tsai, C. L. Lin, C. Lu, G. P. Wang and N. I. Zheludev, *Nat. Commun.*, 2012, **3**, 651.

[28] C. Wyatt Shields IV, C. D. Reyes and G. P. Lopez, *Lab Chip*, 2015, **15**, 1230−1249.

[29] X. C. Li, J. Wu, A. Q. Liu, Z. G. Li, Y. C. Seow, H. J. Huang, K. Xu and J. T. Lin, *Appl. Phys. Lett*., 2008, **93**, 193901.

[30] Y. Yang, A. Q. Liu, L. Lei, L. K. Chin, C. D. Ohl, Q. J. Wang and H. S. A. Yoon, *Lab Chip*, 2011, **11**, 3182−3187.

[31] Y.-C. Chen, Q. Chen and X. Fan, *Lab Chip*, 2016, **16**, 2228−2235.

[32] X. Zhang, W. Lee and X. Fan, *Lab Chip*, 2012, **12**, 3673−3675.

[33] H. Huang, X. L. Mao, S. S. Lin, B. Kiraly, Y. P. Huang and T. J. Huang, *Lab Chip*, 2010, **10**, 2387−2393.

[34] P. M. Hansen, V. K. Bhatia, N. Harrit and L. Oddershede, *Nano Lett.*, 2005, **5**, 1937−1942.

[35] M. T. Carlson, A. J. Green and H. H. Richardson, *Nano Lett.*, 2012, **12**, 1534−1537.

[36] M. Padgett and R. D. Leonardo, *Lab Chip*, 2011, **11**, 1196−1205.

[37] P. B. Johnson and R. W. Christy, *Phys. Rev. B*, 1972, **6**, 4370−4379.

[38] S. Duhr and D. Braun, *Proc. Natl. Acad. Sci. USA*, 2006, **103**, 19678−19682.

[39] D. Erikson, X. Serey, Y. F. Chen and S. Mandal, *Lab Chip*, 2011, **11**, 995−1009.

[40] J. J. Shi, X. L. Mao, D. Ahmed, A. Colletti and T. J. Huang, *Lab Chip*, 2008, **8**, 221−223.

[41] L. K. Chin, J. Q. Yu, Y. Fu, T. Yu, A. Q. Liu and K. Q. Luo, *Lab Chip*, 2011, **11**, 1856−1863.

[42] H. T. Zhao, Y. Yang, L. K. Chin, H. F. Chen, W. M. Zhu, J. B. Zhang, P. H. Yap, B. Liedberg, K. Wang, G. Wang, W. Ser and A. Q. Liu, *Lab Chip*, 2016, **16**, 1617−1624.

[43] Y. H. Zhao, Z. S. Stratton, F. Guo, M. I. Lapsley, C. Y. Chan, S. S. Lin and T. J. Huang, *Lab Chip*, 2013, **13**, 17−24.

[44] T. Li, S. Kheifets, D. Medellin and M. G. Raizen, *Science*, 2010, **324**, 1673−1675.

[45] S. Xiong, A. Q. Liu, L. K. Chin and Y. Yang, *Lab Chip*, 2011, **11**, 1864−1869.

[46] Y. Yang, L. K. Chin, J. M. Tsai, D. P. Tsai, N. I. Zheludev and A. Q. Liu, *Lab Chip*, 2012, **12**, 3785−3790.

[47] J. Q. Yu, W. Huang, L. K. Chin, L. Lei, Z. P. Lin, W. Ser, H. Chen, T. C. Ayi, P. H. Yap, C. H. Chen and A. Q. Liu, *Lab Chip*, 2014, **14**, 3519−3524.

[48] S. Kheifets, A. Simha, K. Melin, T. Li and M. G. Raizen, *Science*, 2014, **343**, 1493−1496.

[49] D. G. Zarlenga, H. A. Larrondo, C. M. Arizmendi and F. Family, *Phys. Rev. E*, 2007, **75**, 051101.

[50] T. Franosch, M. Grimm, M. Belushkin, F. M. Mor, G. Foffi, L. Forro and S. Jeney, *Nature*, 2011, **478**, 85−88.

[51] M. C. Wang and G. E. Uhlenbeck, *Rev. Mod. Phys.*, 1945, **17**, 323−342.

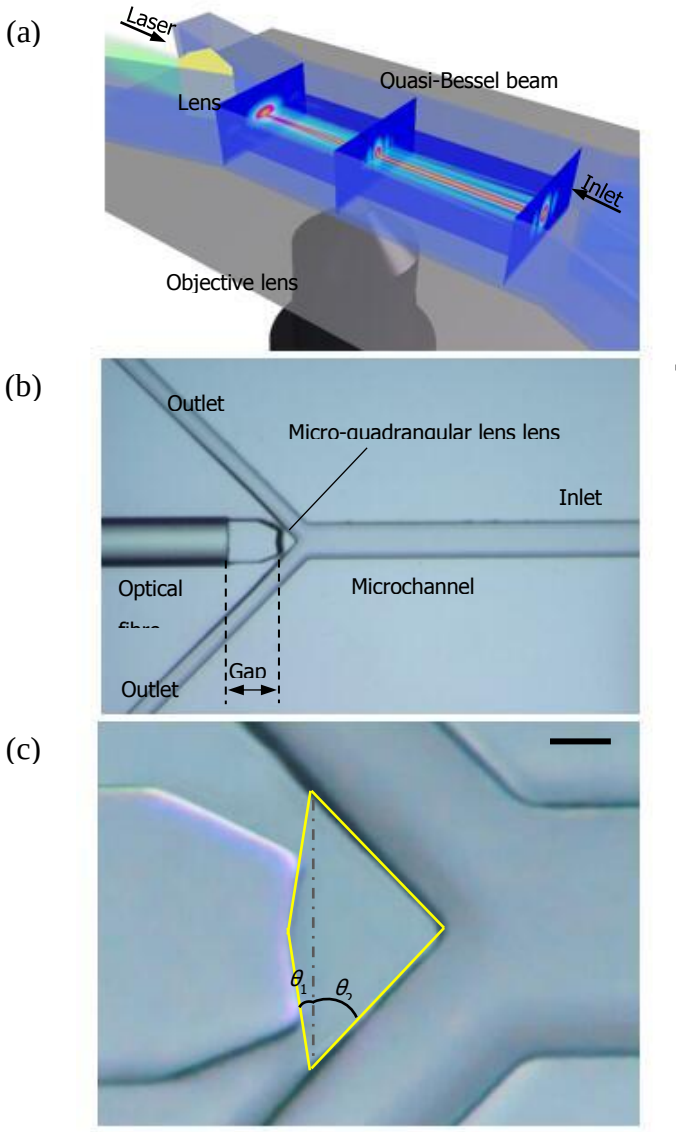

Fig. 1 Design of the system for the high-resolution and multi-scale particle and separation in an optofluidic chip. (a) Schematic illustration of the optofluidic chip. (b) The optofluidic chip was fabricated from PDMS using standard soft-lithography processes. The micro-quadrangular lens is illuminated by the Gaussian beam from the optical fibre. Scale bar equals 100 μm. (c) The micro-quadrangular lens is equivalent to the combination of two prisms with open angles of θ_1 and θ_2. Scale bar equals 20 μm.

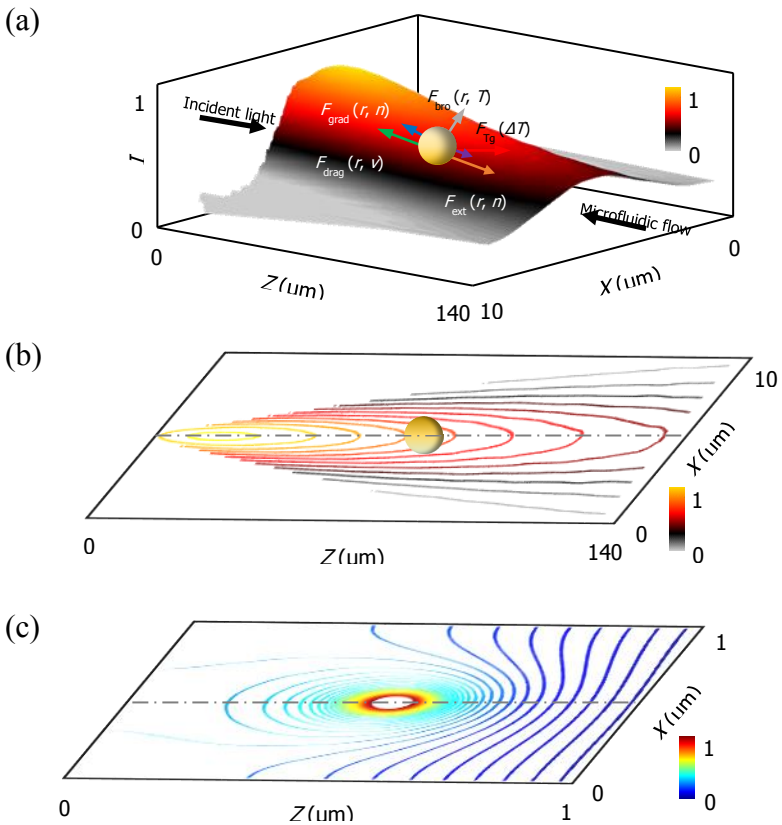

Fig. 2 Analysis of the trapping environment of nanoparticles in an optofluidic chip. (a) Analysis of forces on the gold nanoparticle and (b) the corresponding force contour in the microchannel. (c) Normalised temperature profile around the trapped nanoparticle.

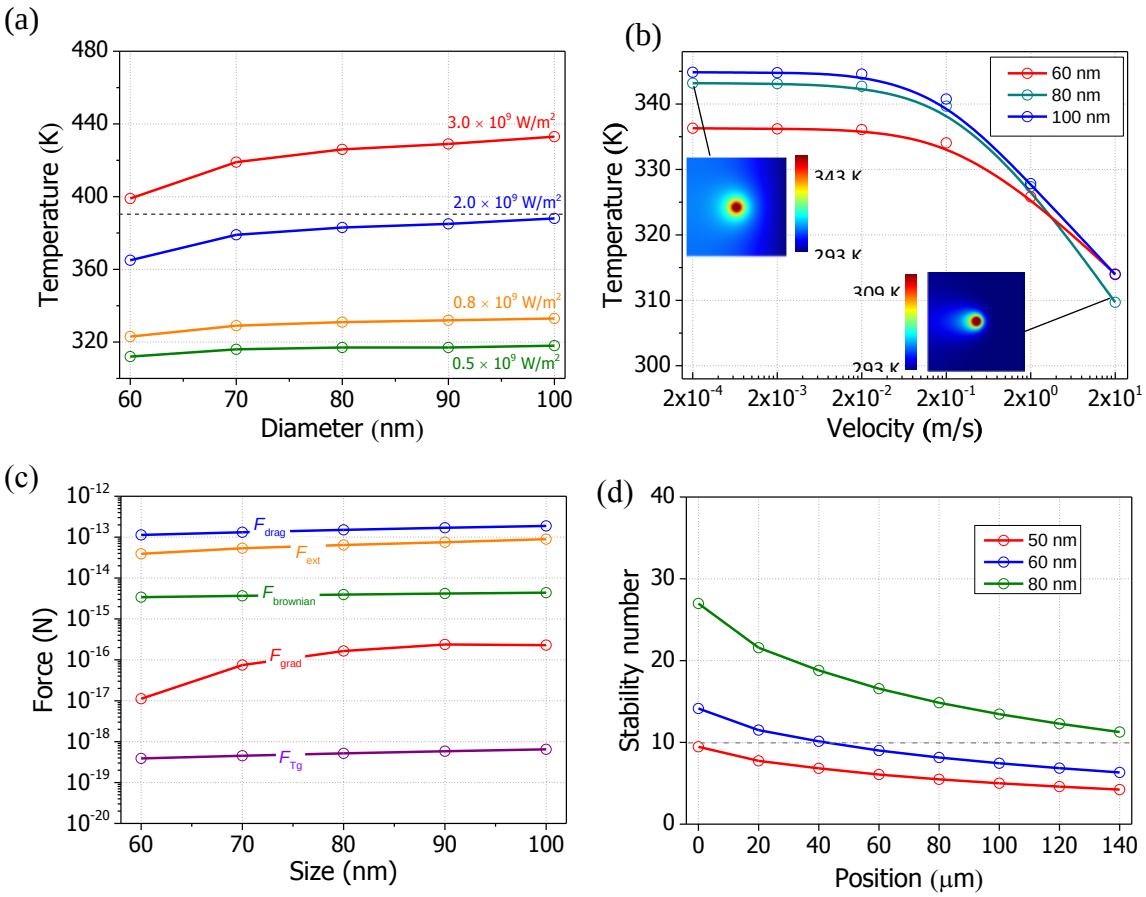

Fig. 3 Simulated temperature, forces and trapping stability of a nanoparticle in the optofluidic chip. (a) Temperatures of the nanoparticle under illumination at different laser intensities. (b) Temperatures of nanoparticles with diameters of 60, 80 and 100 nm under different flow rates. Insets show the temperature profiles surrounding the 80-nm nanoparticle with flow rates of 200 μm/s and 2 m/s. The laser intensity used in the simulation was 1 mW/μm^2. (c) Simulated forces exerted on the nanoparticles in the optofluidic chip. The laser intensity and the temperature used in the calculation are 1 mW/μm^2 and 373 K, respectively. (d) Stability numbers of the nanoparticles at different

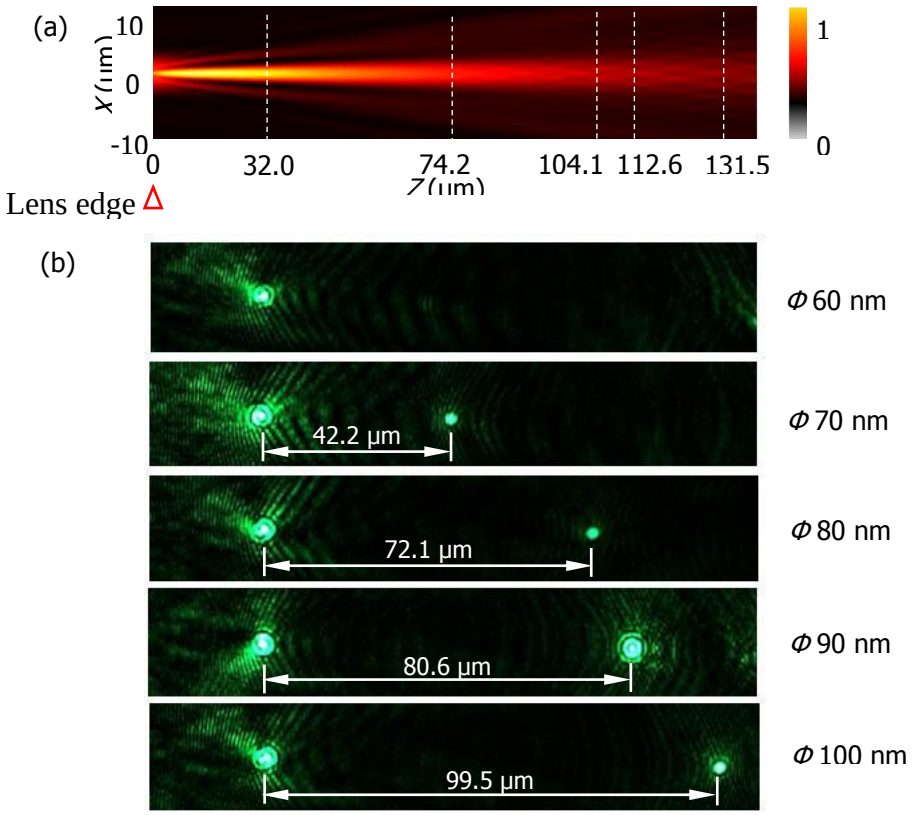

Fig. 4 Trapping of multiple nanoparticles in the microchannel. (a) Light-intensity profile of the quasi-Bessel beam and the trapping positions of different nanoparticles. (b) Trapped nanoparticles with different diameters in the microchannel. The laser power is 400 mW

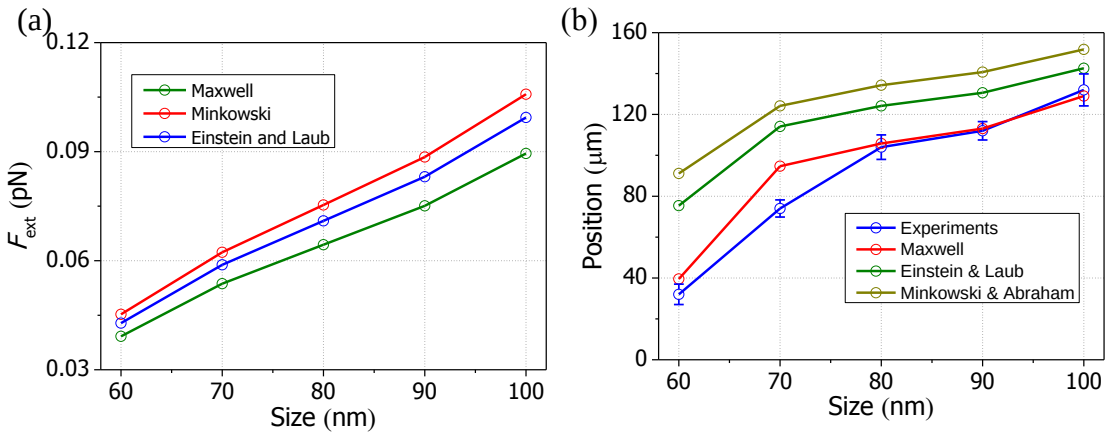

Fig. 5 Comparison of calculated and measured trapping positions of gold nanoparticles (a) Calculated optical extinction forces on different gold nanoparticles. (b) Trapping positions obtained from different Stress tensors and experimental measurement.

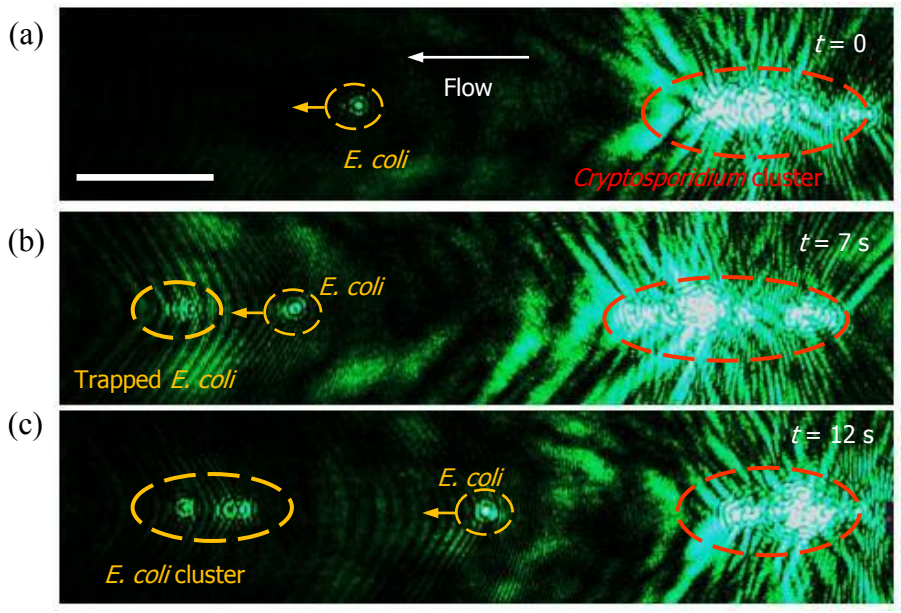

Fig. 6 Separation of *E. coli* and *Cryptosporidium* oocysts in the microchannel. (a) At t = 0, a single *E. coli* moves to the left with the flow. The cluster of *Cryptosporidium* oocysts is trapped on the right side of the microchannel. (b) At t = 7 s, the *E. coli* is trapped on the left side of the microchannel. And another *E. coli* is moving to the left. (c) At t = 12 s, the cluster of *E. coli* is stably trapped. Scale bar equals 40 μm.

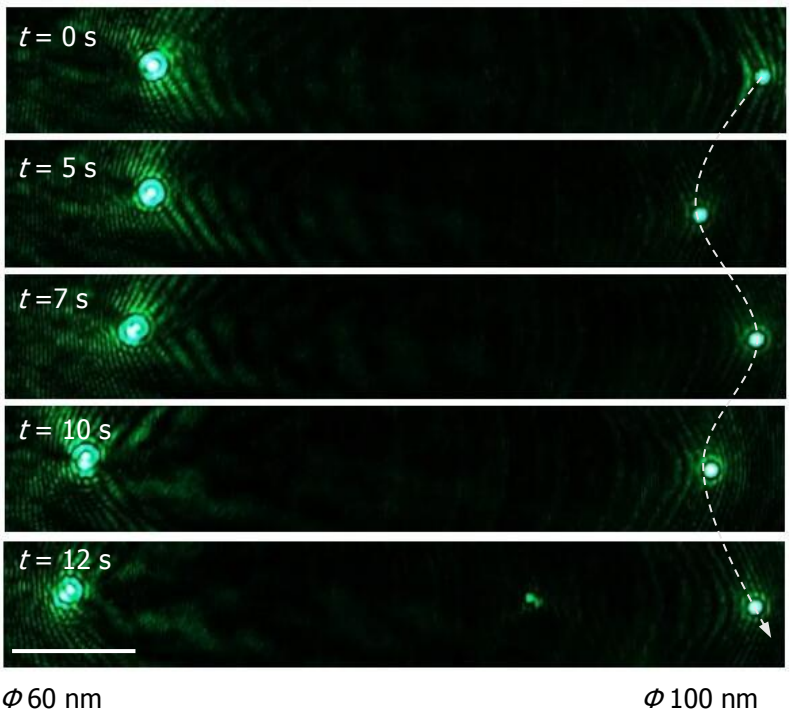

Fig. 7 Experimental observation of microscopic vibration of nanoparticles. Nanoparticles with diameters of 60 and 100 nm vibrate on the left and right sides of the microchannel, respectively. Scale bar equals 15 μm.